Mon. Not. R. Astron. Soc. **386,** 1145–1156 (2008) doi:10.1111/j.1365-2966.2008.13115.x

# VLT photometry in the Antlia cluster: the giant ellipticals NGC 3258 and NGC 3268 and their globular cluster systems⋆

Lilia P. Bassino,[1,2]† Tom Richtler[3]† and Boris Dirsch[3]†

[1]*Facultad de Ciencias Astronómicas y Geofísicas, Universidad Nacional de La Plata, Paseo del Bosque S/N, 1900-La Plata, Argentina*
[2]*Instituto de Astrofisìca de La Plata (CONICET–UNLP), Paseo del Bosque S/N, 1900-La Plata, Argentina*
[3]*Universidad de Concepción, Departamento de Física, Casilla 160-C, Concepción, Chile*

Accepted 2008 February 14. Received 2008 January 22; in original form 2007 August 10

**ABSTRACT**

We present a deep Very Large Telescope (VLT) photometry in the regions surrounding the two dominant galaxies of the Antlia cluster, the giant ellipticals NGC 3258 and NGC 3268. We construct the luminosity functions of their globular cluster systems (GCSs) and determine their distances through the turn-over magnitudes. These distances are in good agreement with those obtained by the SBF method. There is some, but not conclusive, evidence that the distance to NGC 3268 is larger by several Mpc. The GCSs colour distributions are bimodal but the brightest globular clusters (GCs) show a unimodal distribution with an intermediate colour peak. The radial distributions of both GCSs are well fitted by de Vaucouleurs laws up to 5 arcmin. Red GCs present a steeper radial density profile than the blue GCs, and follow closely the galaxies' brightness profiles. Total GC populations are estimated to be about $6000 \pm 150$ GCs in NGC 3258 and NGC $4750 \pm 150$ GCs in NGC 3268. We discuss the possible existence of GCs in a field located between the two giant galaxies (intracluster GCs). Their luminosity functions and number densities are consistent with the two GCSs overlapping in projection.

**Key words:** galaxies: clusters: general – galaxies: elliptical and lenticular, cD – galaxies: individual: NGC 3258 – galaxies: individual: NGC 3268 – galaxies: photometry – galaxies: star clusters.

## 1 INTRODUCTION

The Antlia galaxy cluster has long been overlooked in optical studies despite the fact that it is the nearest cluster after Virgo and Fornax, with a comparable number of members and total mass as the latter (Ferguson & Sandage 1990; Pedersen, Yoshii & Sommer-Larsen 1997; Nakazawa et al. 2000). Its central part consists of two subgroups, each dominated by one of the giant elliptical galaxies NGC 3258 and NGC 3268. This particular structure makes it an even more interesting target, as evidence for interactions between the galaxies in the central cluster region may emerge. However, large differences in the radial velocities between NGC 3268 and several close and bright neighbours suggest a considerable structural depth. We have performed the first CCD study of the stellar population in NGC 3258 and NGC 3268 (Dirsch, Richtler & Bassino 2003a, hereafter Paper I), where the existing literature on the Antlia cluster is summarized.

Afterwards, our study of the galaxy content of this cluster (Smith Castelli et al., in preparation) revealed the presence of numerous low surface brightness galaxies, which had not been identified in a former photographic search carried out by Ferguson & Sandage (1990).

In Paper I, the luminosity and colour profiles of NGC 3258 and NGC 3268, and of their GCSs, were studied on the basis of wide-field Washington photometry. Both GCSs show bimodal colour distributions, but small number statistics prevented the detection of any difference between the radial profiles of the two globular cluster (GC) subpopulations. Unfortunately, these data were not deep enough to reach the turn-over magnitudes (TOMs) of the respective GCS luminosity functions (LFs), which can be used as distance indicators, and it was not possible to estimate new distances. The SBF distances determined by Tonry et al. (2001) are the only ones available, besides a distance estimation via the Hubble flow (Hopp & Materne 1985).

A recent study of GCSs in eight brightest cluster galaxies by Harris et al. (2006) includes both Antlia ellipticals. On the basis of (*B*, *I*) photometry obtained with the ACS/WFC camera from the *Hubble Space Telescope* (field of view of $\approx 3.4 \times 3.4$ arcmin$^2$), they focus on the two-colour data and metallicity distributions. Harris et al. confirm our results from Paper I that the GC colour distributions

⋆Based on observations carried out at the European Southern Observatory, Paranal (Chile). Programme 71.B-0122(A).

†E-mail: lbassino@fcaglp.unlp.edu.ar (LPB); tom@mobydick.cfm.udec.cl (TR); borischacabuco@yahoo.co.uk (BD)

© 2008 The Authors. Journal compilation © 2008 RAS

in these Antlia galaxies are bimodal. They found a trend in the sense that brightest blue GCs seem to become redder with increasing luminosity. With regard to the radial projected distribution, Harris et al. also show that red GCs are more centrally concentrated than blue ones.

In this new investigation with VLT data, we determine GC luminosity functions (GCLFs) and, through their turn-overs, the distance estimates for the dominant Antlia ellipticals. We study the characteristics of the different GC subpopulations in each galaxy, and compare them to the galaxies' light profiles. The total GC populations are also calculated. In addition, the GCSs near the giant elliptical galaxies are compared to the cluster population in a field further away, about 100 kpc from both galaxies (the 'intracluster' field). One goal of this comparison is to search for intracluster GC candidates, i.e. GCs that may be unbound to a parent galaxy, but are instead moving freely in the potential well of the cluster (e.g. West et al. 1995).

This paper is organized as follows. Section 2 describes the observations, the adopted criteria for the GC candidates' selection, and the completeness and reddening corrections. In Section 3 we analyse the results from the four observed fields and perform the distance calculations. Section 4 deals with the galaxies' properties, and Sections 5 and 6 with those of their GCSs. A discussion of the results is presented in Section 7 and, lastly, the conclusions and a summary are provided in Section 8.

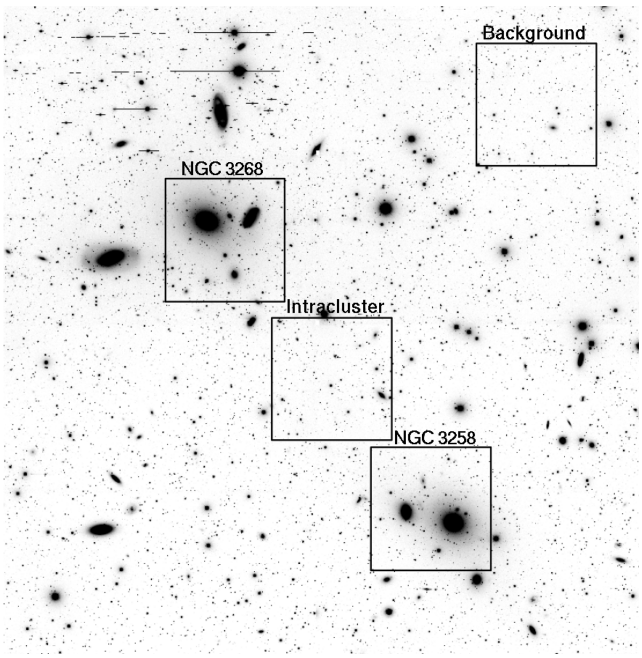


**Figure 1.** The positions of the four observed FORS1 fields are shown. The underlying image is the *R* MOSAIC image that has been used in Paper I. North is up and east is to the left.

## 2 OBSERVATIONS AND REDUCTIONS

### 2.1 Observations

Bessel *V* and *I* imaging was obtained for four fields in the Antlia cluster during 2003 March 27–28, with FORS1 at the VLT UT1 (Antu) telescope (Cerro Paranal, Chile). This camera is equipped with a 2048 × 2048 pixels$^2$ CCD chip, which provides an image scale of 0.2 arcsec pixel$^{-1}$ and a field of view of 6.8 × 6.8 arcmin$^2$ (about 60 × 60 kpc$^2$ at the Antlia distance).

The positions of the fields are shown in Fig. 1 and basic data are listed in Table 1. The labels of the fields (see Fig. 1) were selected as follows: 'NGC 3258' and 'NGC 3268' for those that are located on the dominant galaxies, 'intracluster' for the field placed in between them, and 'background' for the field located close to the border of the MOSAIC field, used to correct for the contamination by the background. For the four fields, three images with exposure times of 100/200 s each plus five images with exposure times of 300/700 s each were obtained in the *V*/*I* bands, respectively. In all cases, short exposures of 10 s were also taken to avoid saturation problems. The seeing was excellent (Table 1).

### 2.2 Photometry and point sources selection

The photometry has been done with DAOPHOT II within IRAF, with the tasks DAOFIND, PSF and ALLSTAR. In the final *V* and *I* images, a second-order variable point source function (PSF) was derived using an average of 30 evenly distributed stars per frame. The aperture corrections were estimated for each field and each band. The point sources selection was performed using the $\chi$ and sharpness parameters calculated by ALLSTAR.

The first night, in which NGC 3258 and NGC 3268 were observed, was photometric and the data were calibrated with the zero-points, airmasses and colour coefficients provided by the European Southern Observatory (ESO). As standard stars used by ESO are taken from Landolt (1992), we obtain magnitudes and colours in the Johnson/Cousins system. For the second night, no zero-point is given and the flux measurements (available on the ESO web site) indicated possible presence of clouds until 2 UT. Our observations started at 3:25 ('intracluster' field) and 5:32 ('background' field), respectively. Hence, it is highly probable that the night has been photometric during this time, so we applied the same zero-points as for the first night (the daily scatter of the zero-point is relatively small). The quality of this latter 'calibration' can be quantified using the Washington ($C$, $T1$) photometry from Paper I: the two-colour diagrams ($V - I$) versus ($C - T1$) are shown in Fig. 2 for the point sources in the 'intracluster' and the 'background' fields. The median values, indicated by solid lines, are compared with those from the NGC 3258 and NGC 3268 fields shown with the dashed lines. In the colour range $(C - T1) > 2$ the point sources are dominated by foreground stars that have identical characteristics in all four fields. No shift that would indicate a photometric zero-point difference can be seen in this colour range. The differences for $(C - T1) < 2$ are due to the presence/absence of GCs and their different properties in the different fields. Similarly, the photometric calibration of the $V$ filter has been checked with a ($V - T1$) versus ($C - T1$) diagram (not shown), resulting in the same conclusions.

The absolute calibration of the first night has been checked using the galaxy aperture photometry for NGC 3258 and NGC 3268 compiled by Prugniel & Siemen (1996). It is shown for NGC 3268 in Fig. 3. The difference of the means are $\Delta V = -0.03 \pm 0.02$, $\Delta I = 0.04 \pm 0.03$ and $\Delta(V - I) = -0.06 \pm 0.03$ (negative values mean that our measurements are brighter/bluer). For NGC 3258 we find: $\Delta V = -0.06 \pm 0.02$, $\Delta I = 0.00 \pm 0.01$, $\Delta(V - I) = -0.06 \pm 0.02$. The overall agreement is good, however, we measure the galaxies about 0.05 mag bluer in ($V - I$).

We modelled the galaxy light of the two ellipticals with the ELLIPSE task within the IRAF/STSDAS/ISOPHOTE package (Jedrzejewski 1987). Since the fields are rather crowded, we first masked the brightest stars by hand and then used five iterations with a 3$\sigma$ clipping. This

**Table 1.** Basic data of the observations. Position of the field: columns (2) and (3); date of observation: column (4); seeing on the final, combined $V$ image: column (5); reddening towards the centre of the field according to Schlegel, Finkbeiner & Davis (1998): column (6).

| Field | RA (J2000) | Dec. (J2000) | Date | Seeing (arcsec) | $E(B-V)$ |
|---|---|---|---|---|---|
| NGC 3258 | $10^{h}29^{m}00\overset{s}{.}0$ | $-35°35'28\overset{''}{.}3$ | 3/27/2003 | 0.53 | 0.084 |
| NGC 3268 | $10^{h}29^{m}54\overset{s}{.}5$ | $-35°20'27\overset{''}{.}4$ | 3/27/2003 | 0.54 | 0.101 |
| Intracluster | $10^{h}29^{m}27\overset{s}{.}6$ | $-35°28'20\overset{''}{.}6$ | 3/28/2003 | 0.64 | 0.090 |
| Background | $10^{h}28^{m}31\overset{s}{.}7$ | $-35°12'51\overset{''}{.}1$ | 3/28/2003 | 0.56 | 0.091 |

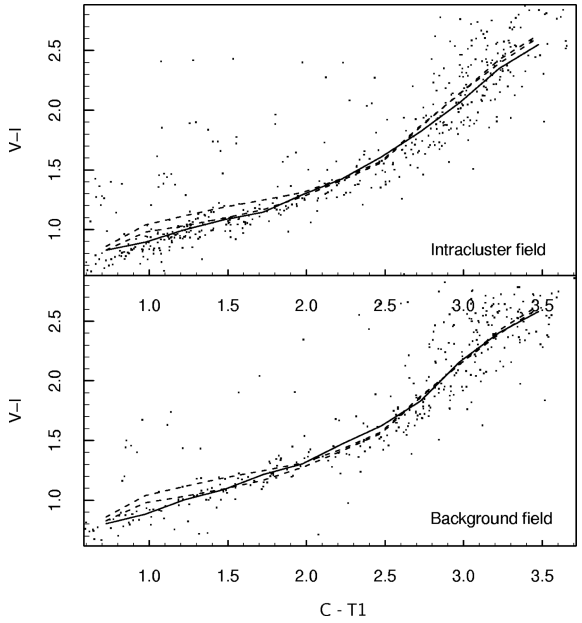


**Figure 2.** Two-colour diagrams for the 'intracluster' and 'background' fields, for the point sources for which $V$, $I$ photometry from this paper and $C$, $T1$ photometry from Paper I are available. The solid lines show the median relation in the respective fields. The dashed lines show the relation in the NGC 3258 and NGC 3268 fields, observed under photometric conditions. The comparison for $(C-T1) > 2$ verifies that in both fields the applied calibration is correct, while for $(C-T1) < 2$ it is affected by the different properties of the GCSs in the four fields (see text).

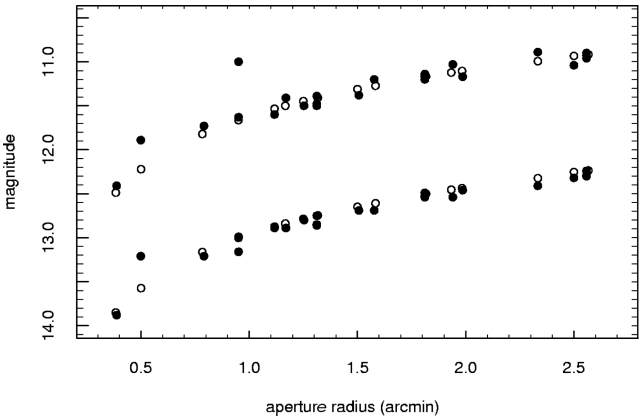


**Figure 3.** Aperture photometry of NGC 3268 in $I$ (upper branch) and in $V$ (lower branch) for our data (open circles) and for data from the compilation of Prugniel & Siemen (1996) (solid circles).

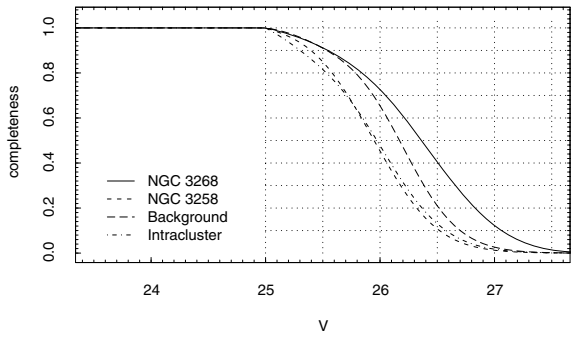


**Figure 4.** Overall completeness for the four fields.

procedure can lead to an underestimation of the total surface brightness; however, the main goal was to obtain a good fitting galaxy model, which characterizes the radial profile, the ellipticity and the position angle (PA) (see Section 4).

### 2.3 Completeness

We performed a standard completeness test by adding $10 \times 1000$ artificial stars, based on the PSF and uniformly distributed, to the four images. We then determined the probability that these stars were retrieved in an analysis analogous to the one performed on the pure science images. We found that the completeness does not vary within the colour range relevant for the GCs ($0.75 < V-I < 1.4$). It is however, spatially dependent: the completeness limit is lower for areas nearer to bright galaxies. This effect is considered later on.

When one compares the completeness curves shown in Fig. 4 with the colour–magnitude diagrams (CMDs) in the next section, a discrepancy becomes apparent, particularly in the NGC 3258 and 'intracluster' fields. The completeness appears to be dropping faster in these observed fields compared to the prediction of the completeness calculations. For further illustration, we refer to Fig. 5 in which the result of the completeness calculation in that field is compared to the true (shifted in $V-I=1.5$) CMD. It appears that the fraction of faint artificial stars is higher than that of the true ones. We have no final explanation for this difference. However, the artificial stars are not concentrated towards the galaxies, so they will on the average have a lower underlying surface brightness and thus will be more sensitive to incompleteness effect than the real GCs. We want to emphasize that the shape of the completeness curve for low luminosities is mainly determined by the used $\chi$ and sharpness point source selection criteria. These criteria have been adjusted using the completeness calculations, but apparently true stars in the NGC 3258 field behave *worse* when the PSF is fitted than the artificial stars. We want to note that a similar apparent difference can also be seen in other works, e.g. Ostrov, Forte & Geisler (1998).

© 2008 The Authors. Journal compilation © 2008 RAS, MNRAS **386,** 1145–1156

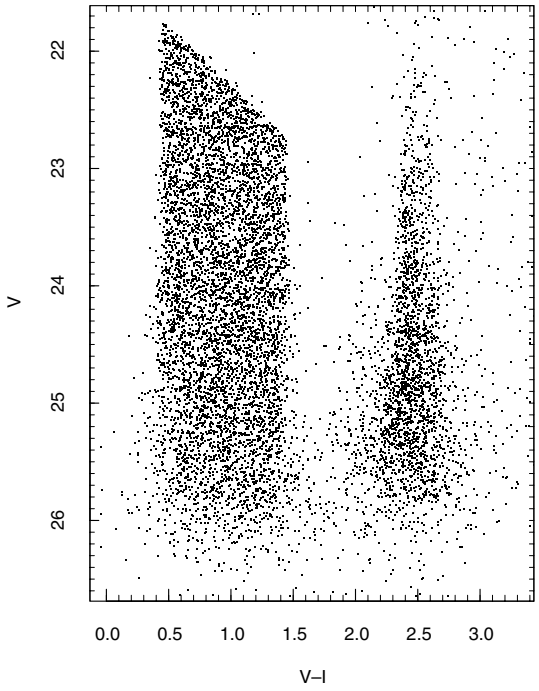


**Figure 5.** CMD of the GCs around NGC 3258 compared to the CMD of the added stars used for the completeness calculation. The former ones are shifted in $V - I$ by 1.5 magnitudes redwards to allow an easy comparison.

Due to this uncertainty, we will only use objects brighter than the limit set by a 70 per cent completeness for the analysis of the GCLFs. Despite this cautious approach, we are reaching at least 1.5 mag deeper than in Paper I.

### 2.4 Reddening correction

We use a conversion factor of $E(V - I)/E(B - V) = 1.2$ (Dean, Warren & Cousins 1978; Stanek 1996) and the adopted values for $E(B - V)$ are listed in Table 1. We want to emphasize that the later conversion factor is adequate for a Kron–Cousins *I* filter. Later on we also compare our results to those obtained with Washington photometry (Paper I); for this system the conversion factor is $E(C - T1)/E(B - V) = 1.97$ (Harris & Canterna 1977).

It can be seen from Table 1 that the reddening towards the different fields varies from $E(B - V) = 0.08$ to 0.10, which corresponds to a range in $E(V - I) = 0.10$–0.12. As already stated in Paper I, the *IRAS* map towards the Antlia cluster is very patchy. In the present work, we are using smaller fields than in Paper I so we will apply reddening corrections according to the individual values listed in Table 1. However, these reddening uncertainties should be kept in mind when comparing results between the different fields.

## 3 THE FOUR FIELDS COMPARED

### 3.1 Colour–magnitude diagrams and colour distributions

The CMDs, corrected by reddening, of the point sources in the four fields are shown in Fig. 6. The GCs are found in the colour range $0.75 < (V - I) < 1.4$. It is already discernible that NGC 3268 has a larger fraction of red clusters than NGC 3258, which extend to redder colours. In the 'intracluster' field mainly blue GCs are detected.

The (reddening corrected) colour distributions of the points

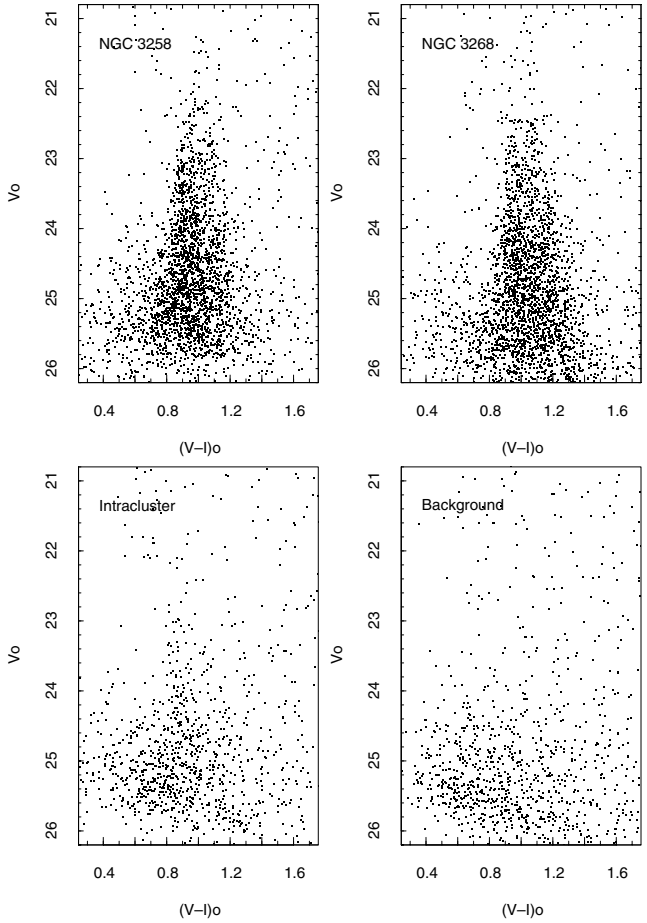


**Figure 6.** CMDs of all point sources in the four studied fields. The GCs can be seen in the colour ranges $0.75 < (V - I) < 1.4$ in the NGC 3258 and NGC 3268 fields and $0.8 < (V - I) < 1.2$ in the 'intracluster' field. The faint, blue objects that dominate the 'background' field are predominately background galaxies.

sources brighter than $V = 25.7$ are shown in Fig. 7 for the four fields, with different vertical scales. The mean colour of the GCs in NGC 3258 is bluer than of those in NGC 3268, which can also be seen in Fig. 6 and in $(C - T1)$ (Paper I). In Paper I a bimodal colour distribution was clearly discernible for the GCSs of both elliptical galaxies. It is not as apparent in these new observations, due to the roughly two times lower metallicity sensitivity of the $(V - I)$ colour compared to the $(C - T1)$ colour, though bimodality is already visible in Fig. 6. A KMM test based on the code of Ashman, Bird & Zepf (1994) gives *p*-values smaller than 0.001 for the colour distributions of both GCSs. These low *p*-values indicate that two Gaussians give a better fit the colour distributions than a single Gaussian. The bimodality in both GCS colour distributions is also clearly established by the $(B - I)$ colour histograms depicted by Harris et al. (2006) in their fig. 9. The results of a two-Gaussian fit, based on a non-linear least-squares code, are tabulated in Table 2. We recall that, in massive early-type galaxies, the most common values are $(V - I) = 0.95 \pm 0.02$ and $1.18 \pm 0.04$ for the blue and red peaks, respectively (Larsen et al. 2001, see also Kundu et al. 2001).

The total fraction of red GCs that we obtain is $24 \pm 5$ per cent in NGC 3258, and $38 \pm 7$ per cent in NGC 3268. Rhode & Zepf (2001, 2004) found proportions of ≈40 per cent of red GCs in their wide-field studies of NGC 4427 and 4406, respectively. With regard

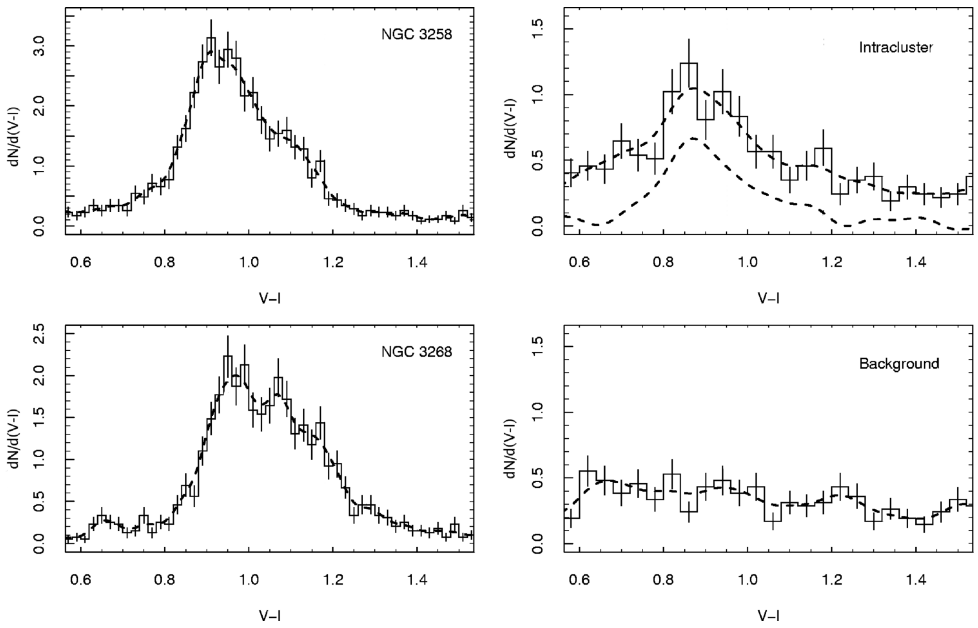


**Figure 7.** Colour distributions of the points sources brighter than $V$=25.7 for all the studied fields. The lower dashed line in the 'intracluster' field is the colour distribution after the background subtraction.

**Table 2.** Results of two-Gaussian fittings to the colour distributions of the elliptical galaxies GCSs.

| | Blue population | | | Red population | | |
|---|---|---|---|---|---|---|
| | Fraction (per cent) | Peak colour | Width | Fraction (per cent) | Peak colour | Width |
| NGC 3258 | $76 \pm 3$ | $0.93 \pm 0.01$ | $0.10 \pm 0.01$ | $24 \pm 5$ | $1.13 \pm 0.01$ | $0.06 \pm 0.01$ |
| NGC 3268 | $62 \pm 14$ | $0.98 \pm 0.02$ | $0.08 \pm 0.01$ | $38 \pm 7$ | $1.16 \pm 0.04$ | $0.10 \pm 0.02$ |

to the 'intracluster' field, we only fit one Gaussian to the data and find $(V-I) = 0.89 \pm 0.02, \sigma = 0.09 \pm 0.02$ for the peak position and the width, respectively.

In our studies on GCSs of the Fornax cluster galaxies (Dirsch et al. 2003b; Bassino, Richtler & Dirsch 2006b), we have found that the limit between blue and red GCs is at $(C-T1) = 1.45$–$1.55$. By means of the comparison $(V-I)$ versus $(C-T1)$ depicted in Fig. 2, we estimate this colour limit as $(V-I) = 1.05$, which will be adopted in the rest of this paper and agrees with the one used by Larsen et al. (2001).

### 3.2 The luminosity functions

The LFs of all objects in the cluster colour range $[0.75 < (V-I) < 1.4]$ are plotted for each of the four fields in the upper panel of Fig. 8 while the completeness corrected and background subtracted LFs are shown in the lower panel. In the following discussion we will only consider the GCLFs up to a limiting magnitude where the completeness is higher than 70 per cent, which is $V = 25.7$ for NGC 3258 and the 'intracluster' fields. The NGC 3268 and the 'background' fields are deeper (70 per cent completeness is reached at $V = 26$ and 25.9, respectively) but, as a background correction is required for the further analysis, only point sources brighter than $V = 25.9$ in the NGC 3268 field will be used.

For an old cluster system the LF, when counted in magnitudes, is usually close to a Gaussian. The peak value – TOM – corresponds to a peak in the mass distribution when counted in logarithmic bins, which has been found to be universal for old cluster populations. Therefore, the GCLF can be employed for distance determinations. Jordán et al. (2007) have performed the largest study of GCLFs in early-type galaxies to date (see also Jordán et al. 2006), within the ACS Virgo Cluster Survey. They have fitted two models to the LFs: a Gaussian, which is the standard model, and an 'evolved Schechter function' that takes into account the dynamical processes that destroy the GCs, particularly the low-mass ones. Jordán et al. have shown that for bright galaxies both functions provide similar good fits while the largest differences arise at the low-mass (low-luminosity) end of the GCLF of faint galaxies. In our case, we are dealing with bright galaxies and do not reach the low-mass end of the LFs, so it seems seem appropriate to use Gaussian functions to describe the GCLFs. Furthermore, a t5 function has also been used to fit GCLFs (e.g. Harris 2001; Richtler 2003) but, as no systematic differences in the TOMs have been reported when using these functions instead of Gaussians (Larsen et al. 2001), we finally adopt the Gaussian model to fit the histograms, with bins of 0.15 mag.

Several studies revealed that red and blue cluster populations have different TOMs (M 87: Elson & Santiago 1996; Kundu et al. 1999; Jordán et al. 2002, NGC 4472: Puzia et al. 1999, sample of 15 early-type galaxies: Larsen et al. 2001, M 104: Spitler et al. 2006) which is mainly due to the metallicity dependent mass-to-light ratio (Ashman, Conti & Zepf 1995). Hence, we study the GCLFs of the total, the red and the blue GC populations.

In the lower panel of Fig. 8 a TOM can be clearly seen for NGC 3258 and the 'intracluster' field. For NGC 3268 the situation is slightly more complicated but, as it is the deepest image, a TOM can be also estimated for NGC 3268. The results are tabulated, for

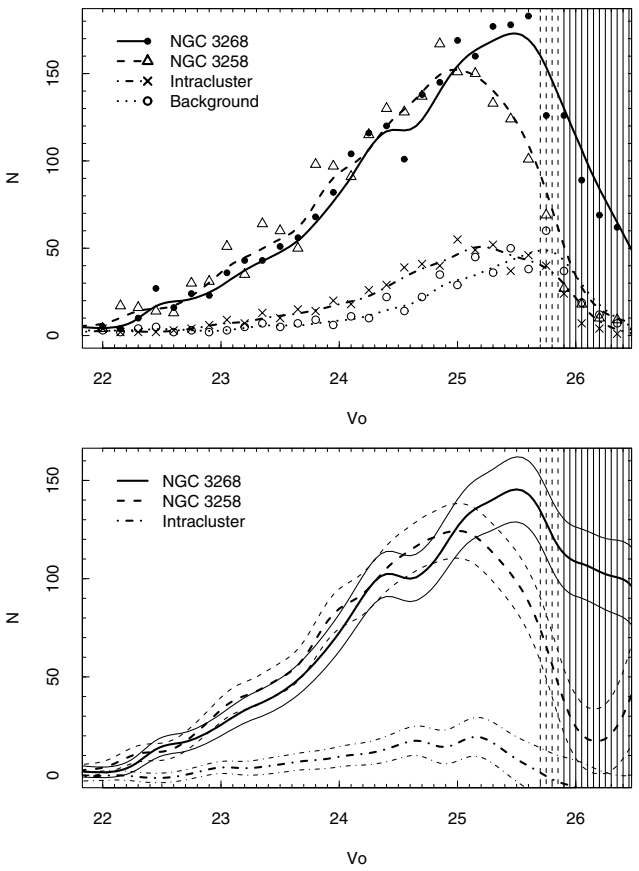


**Figure 8.** Upper panel: Raw LFs of all point sources in the GC colour range $[0.75 < (V - I) < 1.4]$ for the four studied fields. The shaded areas show the luminosity ranges where the counts become uncertain because of the declining completeness ($V = 25.7$ is the limit for the NGC 3258 and 'intracluster' fields, and $V = 25.9$ for the NGC 3268 field). Lower panel: Completeness corrected and background subtracted LFs of all point sources in the GC colour range. The respective shaded bins are not included in the respective fitting LFs (see text). Thinner lines give the corresponding errors, calculated on the basis of the Poisson uncertainties of the raw and background counts, and the effect of the incompleteness.

three radial subsamples, in Table 3. For the 'intracluster' field no TOM for a red subsample has been determined due to poor number statistics.

As can be seen from Table 3, the results for the red GCs show larger errors, particularly in the outer radial subsample (2.3–6 arcmin) where, as will be shown in Sections 5 and 6, these clusters are less numerous. The determined TOMs are radially independent within the errors, as has already been shown in other galaxies (M 87: McLaughlin 1994; Harris, Harris & McLaughlin 1998; Kundu et al. 1999; Jordán et al. 2007, the Milky Way: Harris 2001, M 49: Jordán et al. 2007). However, the TOMs depend on the colour of the GC sample: blue GCs have a brighter TOMs than red ones. Therefore, the red TOMs are also much poorer defined because of their faintness. The difference between the red and the blue TOMs, calculated with the results from the inner radial subsample where the red TOMs are better defined, is $0.53 \pm 0.26$ for NGC 3258 and $0.25 \pm 0.17$ for NGC 3268. These differences agree, within the errors, with those reported by Larsen et al. (2001), but they are not accurate enough (particularly due to the errors in the red TOMs) to drive further conclusions.

### 3.3 The distances towards NGC 3258, NGC 3268 and the 'intracluster' field GCs

In order to determine distances to the galaxies, we use the TOMs of the entire GC populations, estimated over the whole radial range, and adopt as universal absolute TOM $M_{V_0} = -7.46 \pm 0.18$. This universal TOM was determined by Richtler (2003), as a weighted average of the TOMs of the Milky Way and M31 (respectively Harris 2001; Barmby, Huchra & Brodie 2001). It is quite similar to the TOM recently derived for the Milky Way GCLF by Jordán et al. (2007) ($M_{V_0} = -7.5 \pm 0.1$).

Here are our results, where the errors in the distance moduli include the errors of the Gaussian fittings and the adopted universal TOM:

$$(m - M)(\text{NGC } 3258) = 32.42 \pm 0.19;$$
$$(m - M)(\text{NGC } 3268) = 32.81 \pm 0.20.$$

For NGC 3258 and NGC 3268 Tonry et al. (2001) determined distance moduli of $32.53 \pm 0.27$ and $32.71 \pm 0.25$, respectively, which agree well with our measurements.

With regard to the GC population located in the 'intracluster' field, mainly blue GCs (see Fig. 7), it seems more interesting to calculate its distance relative to both giant galaxies than to obtain an absolute estimation. Such relative distance may be estimated comparing the TOMs that are calculated using only blue globulars, over the whole radial range. These TOMs, depicted in Table 3, are $V$=24.81, 25.06 and 24.87 for the NGC 3258, NGC 3268 and 'intracluster' fields, respectively. Assuming an universal absolute TOM for the blue GC population too, the distance to the GCs of the 'intracluster' field is in the middle of those of the galaxies, further than NGC 3258 but closer than NGC 3268.

Summarizing, we find that NGC 3268 seems to be further away than NGC 3258 and that the TOM of the 'intracluster' field GCs suggests that they are located in between both galaxies, as expected if most of the GCs in the 'intracluster' field are part of both galaxies GCSs.

**Table 3.** $V$-band TOMs and width of the Gaussian fittings to the GCLFs; for details see text.

| | | All GCs | | Blue GCs | | Red GCs | |
|---|---|---|---|---|---|---|---|
| | Radial range (arcmin) | $V$-TOM | $\sigma_V$ | $V$-TOM | $\sigma_V$ | $V$-TOM | $\sigma_V$ |
| NGC 3258 | 0.8–2.3 | $24.98 \pm 0.08$ | $1.10 \pm 0.07$ | $24.84 \pm 0.09$ | $1.08 \pm 0.09$ | $25.37 \pm 0.24$ | $1.17 \pm 0.18$ |
| | 2.3–6 | $24.91 \pm 0.12$ | $1.09 \pm 0.12$ | $24.78 \pm 0.12$ | $0.97 \pm 0.13$ | $25.59 \pm 0.62$ | $1.48 \pm 0.41$ |
| | 0.8-6 | $24.96 \pm 0.07$ | $1.10 \pm 0.07$ | $24.81 \pm 0.09$ | $1.04 \pm 0.09$ | $25.83 \pm 0.49$ | $1.46 \pm 0.28$ |
| NGC 3268 | 0.8–2.3 | $25.36 \pm 0.09$ | $1.21 \pm 0.08$ | $25.18 \pm 0.13$ | $1.31 \pm 0.13$ | $25.43 \pm 0.11$ | $1.06 \pm 0.10$ |
| | 2.3–6 | $25.49 \pm 0.15$ | $1.18 \pm 0.12$ | $24.99 \pm 0.09$ | $0.96 \pm 0.10$ | $26.40 \pm 0.80$ | $1.42 \pm 0.37$ |
| | 0.8–6 | $25.35 \pm 0.09$ | $1.22 \pm 0.08$ | $25.06 \pm 0.08$ | $1.12 \pm 0.08$ | $25.79 \pm 0.18$ | $1.22 \pm 0.13$ |
| Intracluster | | $24.79 \pm 0.13$ | $0.77 \pm 0.14$ | $24.87 \pm 0.15$ | $0.80 \pm 0.16$ | | |

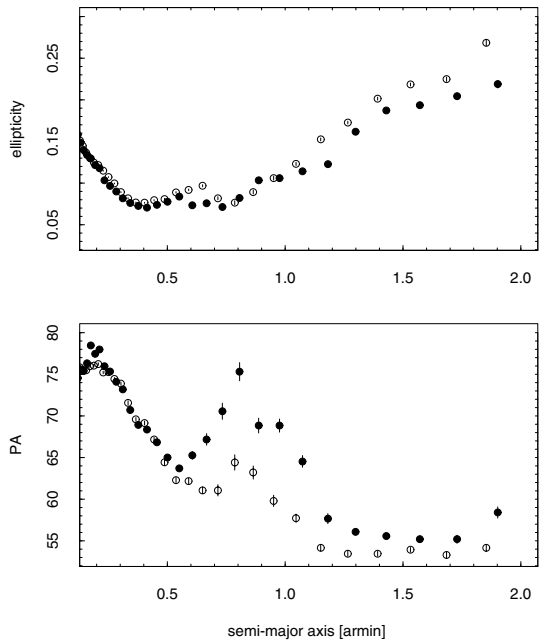


**Figure 9.** NGC 3258: ellipticity (upper panel) and position angle (lower panel) versus semi-major axis, *I* band (solid circles) and *V* band (open circles).

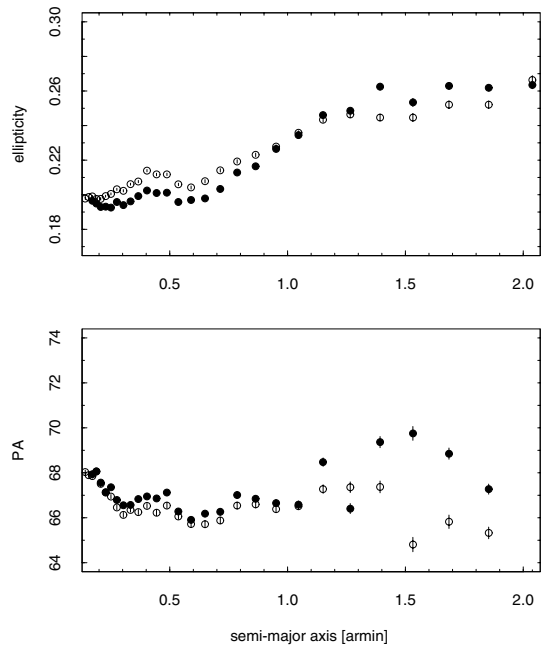


**Figure 10.** NGC 3268: ellipticity and position angle plotted in the same way as in Fig. 9.

As a consequence of the uncertainties, particularly with regards to the reddening towards the Antlia cluster, in the following we will keep a conservative value of 30 Mpc for the distance to the Antlia cluster (1 arcmin will correspond to 8.7 kpc).

## 4 THE STELLAR BODIES OF NGC 3258 AND NGC 3268

We have modelled the light of the two elliptical galaxies, as stated above, by means of the ELLIPSE task within IRAF. The variations of the ellipticity $\epsilon$ and the PA against the semi-major axis, which result from the fits, are shown in Figs 9 and 10 for NGC 3258 and NGC 3268, respectively.

From Fig. 9 we can see that the ellipticity of NGC 3258, in both *V* and *I* bands, shows a slight decline close to the centre, and increases outwards from $\epsilon = 0.07$ at 0.5 arcmin up to $\epsilon = 0.25$ at about 2 arcmin. The PA of the major axis obtained from the isophotal analysis decreases from $\sim 75^\circ$ close to the centre down to $55^\circ$ at about 2 arcmin, with a clear peak around 0.8 arcmin which is more evident in the *I* band. The behaviour of both parameters, $\epsilon$ and PA, are in good agreement with the *BVI* photometry performed by Reid, Boisson & Sansom (1994) and with our previous results from Paper I.

With regard to NGC 3268 (Fig. 10), the ellipticity increases steadily from $\epsilon = 0.2$ at 0.1 arcmin to $\epsilon = 0.26$–$0.27$ at about 2 arcmin, in both *V* and *I* bands. The same results were obtained by Reid et al. (1994) while in the model from Paper I the ellipticity is constant; $\epsilon = 0.2$ out to 2.5 arcmin. The PA remains almost constant, oscillating between $65^\circ$ and $70^\circ$ through the same radial extension, in agreement with both previous studies.

At the centres of both galaxies, there are small dust lanes that can be interpreted as dusty discs. The dusty disc of NGC 3268, with a diameter of 4.4 arcsec, has already been mentioned in Paper I. The smaller one in NGC 3258, with a diameter of 1.8 arcsec, was not visible in the MOSAIC data, but has been detected by De Bruyne et al. (2004).

## 5 THE GCS OF NGC 3258

### 5.1 Radial distribution

The radial density profiles of all GCs, the red $[1.05 < (V - I) < 1.4]$, and the blue $[0.75 < (V - I) < 1.05]$ ones, are shown in Fig. 11 for the GC candidates in NGC 3258 brighter than $V = 25$. Hence, as the TOM for all GCs is around $V = 25$, the number density gives approximately half the total cluster density. In all cases, the errors of the background-corrected distributions include the Poisson uncertainties of the raw and background counts, and the effect of the incompleteness. The profile obtained from the MOSAIC data has been included in the upper panel, together with the VLT ones, as an additional check of the consistency between both observational sets. Typically GC density profiles are fitted by either power laws ($r^{-\alpha}$) or de Vaucouleurs profiles $\{\exp[-a(r^{0.25} - 1)]\}$. Both fits are plotted in Fig. 11, which shows that de Vaucouleurs profiles provide better fits for all the GC selections. All the fits were performed within the range 0.5–5 arcmin and the results are depicted in Table 4.

The exponents of the power-law and de Vaucouleurs fits show that the red clusters present a steeper radial profile than the blue clusters, being more concentrated towards the centre. A similar result, in the sense that a de Vaucouleurs profile provides a better fit, has been found for other giants like, for instance, NGC 4406 (Rhode & Zepf 2004) and NGC 4472 (Rhode & Zepf 2001) in Virgo, or NGC 1399 (Bassino et al. 2006a) in Fornax.

The radial density profile for the red clusters depicted in Fig. 11, has a rather constant and low density for $r > 3$ arcmin (1.4 GCs arcmin$^{-2}$, i.e. about 50 per cent of the background level estimated for the red GCs colour range), suggesting that it is close to reach an end, while the blue clusters clearly extend further than the NGC 3258 field.

We have modelled the light of the two elliptical galaxies, as stated above, by means of the ELLIPSE task within IRAF. The *V* galaxy light profile included in the plots is hardly distinguishable from the

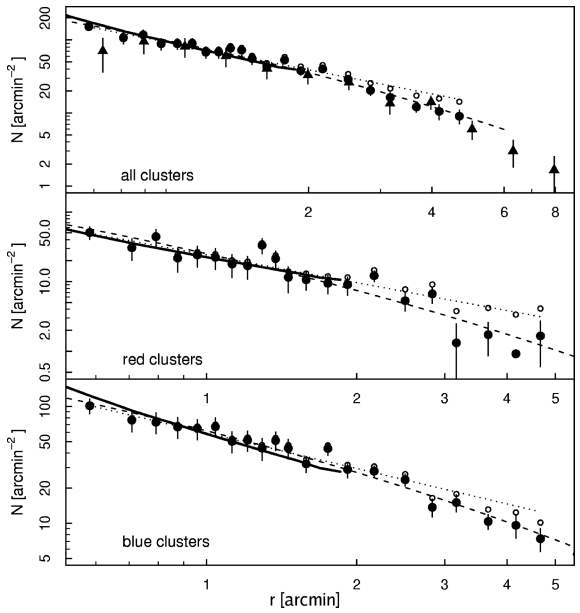


**Figure 11.** NGC 3258: radial density profiles for all (upper panel), red (middle panel) and blue (lower panel) GCs, brighter than $V = 25$. Open circles show the radial distributions uncorrected for background contamination and filled circles the background-corrected distributions. Triangles in the upper panel correspond to the MOSAIC data. Dotted and dashed lines show the power-law and de Vaucouleurs fits, respectively, to the background-corrected data. Thick solid line represents the (arbitrarily scaled) $V$ galaxy brightness profile. (Please note different horizontal and vertical scales.)

**Table 4.** Fits to the radial number density (objects arcmin$^{-2}$) of the whole GCS and two subsamples, up to a limiting magnitude $V$=25, and corrected for contamination and incompleteness. The contribution of the background is relatively low (4.3 objects arcmin$^{-2}$ for the whole GC sample).

| | Power law | de Vaucouleurs |
|---|---|---|
| NGC 3258 | | |
| All clusters | $(83.6 \pm 2.2)\, r^{-1.10\pm0.06}$ | $(87.6 \pm 7.5)\, e^{(-4.8\pm0.2)\,(r^{0.25}-1)}$ |
| Red clusters | $(24.2 \pm 1.6)\, r^{-1.33\pm0.16}$ | $(25.2 \pm 6.3)\, e^{(-6.4\pm0.5)\,(r^{0.25}-1)}$ |
| Blue clusters | $(59.2 \pm 1.4)\, r^{-1.01\pm0.06}$ | $(61.9 \pm 5.2)\, e^{(-4.3\pm0.2)\,(r^{0.25}-1)}$ |
| NGC 3268 | | |
| All clusters | $(70.6 \pm 1.9)\, r^{-1.50\pm0.09}$ | $(68.4 \pm 7.4)\, e^{(-4.7\pm0.2)\,(r^{0.25}-1)}$ |
| Red clusters | $(35.1 \pm 1.8)\, r^{-1.76\pm0.18}$ | $(33.8 \pm 5.2)\, e^{(-5.7\pm0.3)\,(r^{0.25}-1)}$ |
| Blue clusters | $(35.2 \pm 1.4)\, r^{-1.26\pm0.12}$ | $(33.8 \pm 4.9)\, e^{(-3.9\pm0.3)\,(r^{0.25}-1)}$ |

radial density profile for all and red GCs, while slight differences are detectable with respect to the blue cluster profile.

### 5.2 Azimuthal distribution

The ellipticity of the GCS can be determined studying the azimuthal density distribution of GC candidates with respect to the azimuthal angle, that is, a PA measured from north to east. An elliptical GCS causes sinusoidal counts in this diagram: the ellipticity $\epsilon$ and the number density along the major and the minor axes ($N_a$, $N_b$) are related via $\epsilon = 1 - (N_b/N_a)^{1/\alpha}$, where $\alpha$ is the exponent of the radial density distribution ($r^{-\alpha}$).

In the upper panel of Fig. 12 the azimuthal distribution of the NGC 3258 GCS is shown for clusters within 0.5–2 arcmin. A sinusoidal fit to the data results in an ellipticity $\epsilon = 0.21 \pm 0.03$ and a PA of the major axis PA $= 32^\circ \pm 5^\circ$, which are in excellent agreement with those obtained in Paper I.

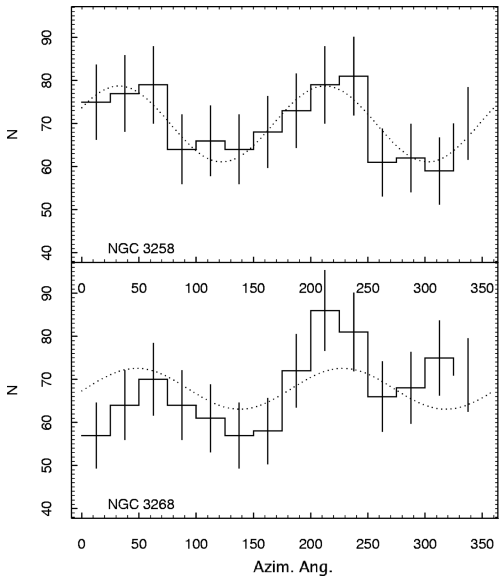


**Figure 12.** Azimuthal number distributions of all cluster candidates brighter than $V = 25.7$ within 0.5–2 arcmin for NGC 3258 (upper panel) and for NGC 3268 (lower panel). The dotted lines show the sinusoidal fits.

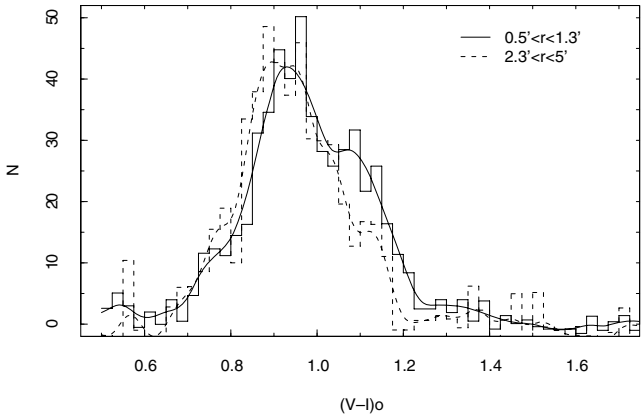


**Figure 13.** Colour distribution of the GCS around NGC 3258 for an inner (solid line) and an outer (dashed line) cluster sample.

### 5.3 Colour distribution

We have shown that red and blue clusters have different radial distribution, hence the colour distribution shows a radial dependence which is shown in Fig. 13. In particular, the presence of red GCs is less noticeable in the outer cluster sample. We have fitted two Gaussians to the histogram data. We find for the inner sample ($0.5 < r < 1.3$ arcmin):

$(V-I)_{\rm peak}({\rm blue}) = 0.94 \pm 0.01,\ \sigma({\rm blue}) = 0.09 \pm 0.01;$
$(V-I)_{\rm peak}({\rm red}) = 1.13 \pm 0.01,\ \sigma({\rm red}) = 0.06 \pm 0.01$

and for the outer sample ($2.3 < r < 5.0$ arcmin):

$(V-I)_{\rm peak}({\rm blue}) = 0.93 \pm 0.01,\ \sigma({\rm blue}) = 0.10 \pm 0.01;$
$(V-I)_{\rm peak}({\rm red}) = 1.14 \pm 0.01,\ \sigma({\rm red}) = 0.02 \pm 0.01.$

No radial dependence of the peak positions can be observed up to our limit in galactocentric radius, that is, about 45 kpc. This result is consistent with the observations in other ellipticals within similar radial ranges (Larsen et al. 2001; Rhode & Zepf 2001; Dirsch, Schuberth & Richtler 2005). In this way, the radial dependence of the colour distribution may be basically explained by the different proportions of the blue and red subpopulations.

We have also tested the colour distribution within different luminosity ranges: bright ($21.5 < V < 23.5$), intermediate ($23.5 < V < 24.5$) and faint ($24.5 < V < 25.5$) samples (the figure is not shown because it is similar to the NGC 3268 one depicted in Fig. 15). For the intermediate and faint samples it is possible to fit two Gaussians. These results show that the blue and red peaks for these luminosity ranges agree with the colours obtained for all GCs together, within the errors (Table 2). However, the red peak of the fainter sample is redder than the red of the intermediate sample ($V - I = 0.93 \pm 0.02/1.09 \pm 0.04$, and $V - I = 0.92 \pm 0.02/1.17 \pm 0.04$, for blues/reds in the intermediate and faint samples, respectively).

For the brighter sample, it is not possible to fit two Gaussians but only one. The peak colour obtained ($V - I = 0.96 \pm 0.01$) is somewhat intermediate between both GC populations. This behaviour has already been detected in other ellipticals that dominate galaxy clusters like e.g. NGC 1399 (Ostrov et al. 1998; Dirsch et al. 2003b), and the sample of eight brightest cluster galaxies from Harris et al. (2006).

## 6 THE GCS OF NGC 3268

### 6.1 Radial distribution

Fig. 14 shows the radial density profiles of all GCs, red and blue ones, for the candidates brighter than $V = 25$ in NGC 3268. In this case, the profiles can be well described by power laws or by de Vaucouleurs profiles. All fits were performed within the range 0.6–5 arcmin and the results are depicted in Table 4. The profile obtained from the MOSAIC data for this GCS has been included in the upper panel, where the difference between the VLT and MOSAIC profiles in the inner region is due to radial incompleteness effects within 0.7 arcmin (see fig. 6 in Paper I).

The slopes of all de Vaucouleurs fits for all GCs (red and blue) agree within the errors with those of the NGC 3258 fits. As in the NGC 3258 GCS, red clusters have a more concentrated distribution than blue clusters. It is apparent from Fig. 14 that the innermost point of the blue GCS profile deviates from the expected position, which is probably due to an underestimation of the completeness correction.

Neither the blue nor the red GC radial density profiles show any feature that can be understood as the spatial limit of the GCS. However, the red profile shows that the zero density level will be reached at a galactocentric radius slightly larger than 5 arcmin.

The galaxy surface luminosity profile shown in Fig. 14 is well traced by the red GCs, but the slope is clearly different from that of the blue GCS profile.

### 6.2 Azimuthal distribution

The azimuthal number counts of the GCs within 0.5–2 arcmin are shown in the lower panel of Fig. 12, from which we derive an ellipticity $\epsilon = 0.09 \pm 0.05$ and a position angle PA $= 48^\circ \pm 20^\circ$. The errors in both parameters are large because the fit is affected by a clear excess in the GC azimuthal distribution, at azimuthal angles between 200°–250°. This excess appears in coincidence with one of the maxima of the sinusoidal fit, and at azimuthal angles that correspond to the direction towards NGC 3258.

It is interesting to note that on the sky, the PA with origin in NGC 3258 that points to the direction of NGC 3268, is 39°. So we confirm the results from Paper I that both GCSs are elongated in a direction close to an axis joining the two galaxies.

### 6.3 Colour distribution

The GC colour distribution is shown in Fig. 15 for three luminosity intervals, within the radial range 0.7–2.3 arcmin. As for NGC 3258, the brightest GCs show a unimodal colour distribution while fainter GCs have bimodal distributions. The distribution also extends to redder colours as we consider fainter GCs.

The two-Gaussian fits show that the blue and red peaks, for the intermediate and faint luminosity ranges, agree with the colours obtained for all GCs together, within the errors (Table 2). However, the red peak of the fainter sample is clearly redder than that of the intermediate sample ($V - I = 0.96 \pm 0.01/1.14 \pm 0.02$, and

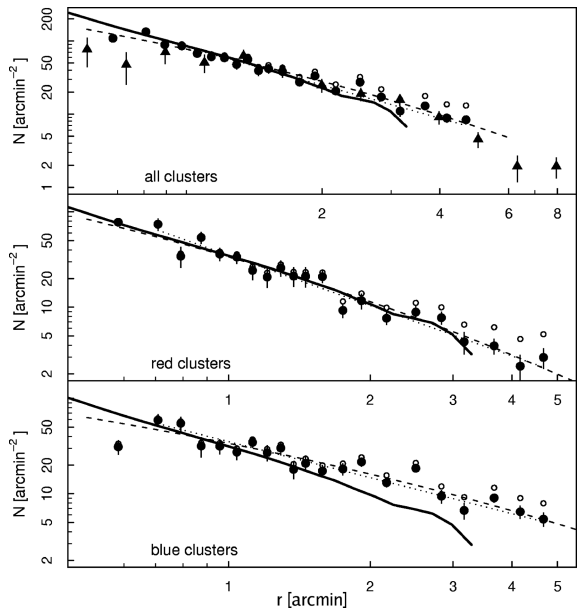


**Figure 14.** NGC 3268: radial density profiles plotted in the same way as in Fig. 11.

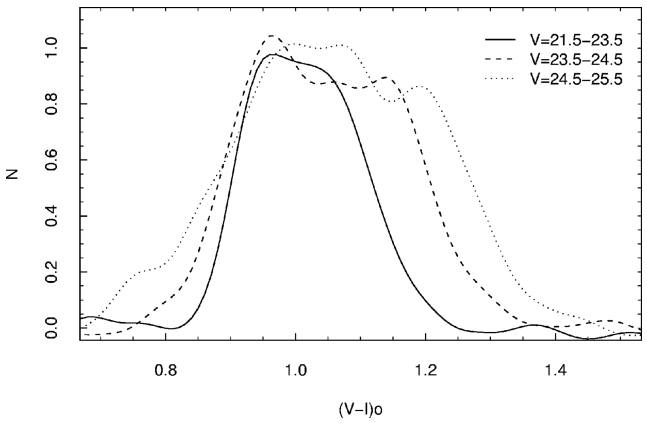


**Figure 15.** Colour distribution of the GCS of NGC 3268 for three different luminosity ranges. The distributions are arbitrarily scaled.

$V - I = 1.02 \pm 0.02/1.23 \pm 0.02$, for blues/reds in the intermediate and faint samples, respectively). Similar trends are present in the NGC 3258 GCS. The peak colour obtained from the single-Gaussian fit to the brightest sample ($V - I = 1.01 \pm 0.01$) is roughly in between both subpopulations.

The colour distributions within different galactocentric radii have also been tested within an inner and outer samples as for NGC 3258. We confirm the radial dependence of the colour distribution because the fraction of red GCs present in the outer sample is smaller than in the inner one. The colours of the blue/red peaks roughly agree, within the errors, with the ones estimated for the whole GC population, but in this case the peaks of the inner sample are redder than those of the outer group ($V - I = 1.02 \pm 0.01/1.21 \pm 0.02$, and $V - I = 0.96 \pm 0.02/1.14 \pm 0.04$, for blue/red peaks in the inner and outer samples, respectively).

## 7 DISCUSSION

### 7.1 The brightest GC candidates

The principal property of the colour distribution of GCs, the bimodality, has been previously found to be absent among the bright GCs of NGC 1399 (Ostrov et al. 1998; Dirsch et al. 2003b) and M87 (Strader et al. 2006). Harris et al. (2006) found the same in their ACS photometry of several central giant ellipticals, including our Antlia galaxies, while this point remained unclear in our previous Washington photometry. Unimodal colour distributions, seem to apply to clusters brighter than approximately $M_V = -10$. Our present photometry reiterates on this finding, shifting the limit between bimodality and unimodality even a bit lower to $M_V = -9$.

It is plausible (and discussed in the literature, see the reviews of Richtler 2006 and Brodie & Strader 2006) that there are several possible formation channels for creating a population of very bright clusters. Stripped galactic nuclei (Bassino, Muzzio & Rabolli 1994), former blue compact galaxies, but also 'normal' formation of massive clusters, perhaps through the merging of smaller subclusters (Fellhauer & Kroupa 2005) are viable candidates or formation histories, which in the centre of a galaxy cluster might occur more frequently than in less dense environments.

### 7.2 Total GC populations and specific frequencies

We can estimate the GC populations performing a numerical integration of the de Vaucouleurs radial density profile, which includes GCs brighter than $V$=25, and doubling the result according to the TOMs of the GCLFs. The external limiting radius of the GCSs is taken as $r = 10$ arcmin following Paper I. In this way, the total GC population of NGC 3258 amounts to $N_{\rm GC} = 6000 \pm 150$ and that of NGC 3268 $N_{\rm GC} = 4750 \pm 150$. In NGC 3258, the red GCs are clearly less numerous than the blues, being the ratio of blues to reds $N_{\rm b}/N_{\rm r} = 4.1$, which is close to the ratio estimated from the colour distribution $N_{\rm b}/N_{\rm r} = 3.2 \pm 0.7$, within the errors (see Table 2). The ratio of blue to red GCs around NGC 3268 is $N_{\rm b}/N_{\rm r} = 1.7$, also close to the ratio derived from the colour distribution $N_{\rm b}/N_{\rm r} = 1.6 \pm 0.8$ (Table 2).

In order to calculate the specific frequency $S_N$ (as defined by Harris & van den Bergh 1981) of both GCSs, we need the $V$-band absolute magnitudes of the host galaxies and number of GCs estimated over the same galactocentric distance. The $R$-band integrated luminosities of the galaxies up to $r = 4$ arcmin can be obtained from Paper I and corrected by absorption in $R$ applying the relation from Rieke & Lebofsky (1985) $A_R/A_V = 0.75$ and the $E(B - V)$ colour excesses depicted in Table 1. We cannot estimate global $S_N$ due to the large uncertainties of the integrated luminosity at larger radii, but we are able to improve the $S_N$ from Paper I (also within $r =$ 4 arcmin) through a more precise determination of the number of GCs. By means of the individual distance moduli estimated in this paper and the colour index $(V - R) = 0.7$ (Paper I) for both galaxies, we obtain absolute luminosities within 4 arcmin $M_V = -21.5 \pm 0.3$ for NGC 3258, and $M_V = -22.2 \pm 0.3$ for NGC 3268, where the errors are calculated with the errors of the apparent magnitudes and of the distance moduli. The corresponding GC populations, up to the same radius, are estimated by numerical integration of the radial density profiles. Finally, the specific frequencies within $r =$ 4 arcmin are $S_N = 8.7 \pm 2.2$ for NGC 3258, and $S_N = 3.7 \pm 0.9$ for NGC 3268. Due to the limited radial range of these calculations, these $S_N$ should be taken as indicative values.

### 7.3 Distances and specific frequencies

The derived distances indicate that NGC 3258 is located somewhat in the foreground with respect to NGC 3268. The TOMs, taken at face value, suggest a difference of 6 Mpc, while the SBF distances are different by 3 Mpc, although the uncertainties would not exclude the same distance. An additional argument is that the 'intracluster' field independently reveals a TOM intermediate between NGC 3258 and NGC 3268 which we expect if the outskirts of the respective GCSs are projected on to each other.

This interpretation is also not without oddities. NGC 3258 has an unusually high specific frequency considering its brightness and, if really in the foreground, would be in a relatively poor environment, at least poorer than that of NGC 3268. Such a high frequency is, however, not unique as we see from the case of NGC 4636 (Dirsch et al. 2005), but extraordinary. A distance modulus of 0.4 mag higher would decrease its specific frequency by a factor of 1.4, making it more common. On the other hand, its TOM is very well sampled, better than that of NGC 3268, so we do not think that the TOM is grossly erroneous.

A few remarks to the group around NGC 3268. The radial velocities of the three neighbour galaxies that are listed in Paper I (NGC 3269, NGC 3271, NGC 3267; these are the only ones for which radial velocities are available), are consistently higher by about 1000 km s$^{-1}$. The morphological appearance suggests NGC 3268 to be the central galaxy of that subgroup of the Antlia cluster. These radial velocities, however, let it appear improbable that NGC 3268 is at rest with respect to that group. Its 'normal' specific frequency also would not qualify it as a 'central' galaxy.

More insight into the structure of the Antlia cluster can only be expected by a radial velocity survey.

### 7.4 Intracluster globular clusters?

With regard to the presence of GCs inside galaxy clusters that are not bound to individual galaxies, observational evidence of their existence have been presented, among others, by Minniti et al. (1998), Kissler-Patig et al. (1999) Bassino et al. (2003), Jordán et al. (2003) and Williams et al. (2007). Besides, numerical simulations on their formation and properties have been performed by Yahagi & Bekki (2005).

In the previous sections we have derived the cluster radial density distribution and fitted de Vaucouleurs laws to the GCSs of NGC 3258 and NGC 3268. We now take these fits, extrapolate them beyond the observed 5 arcmin, and compute the combined cluster density along the connecting axis between the two galaxies. The results for

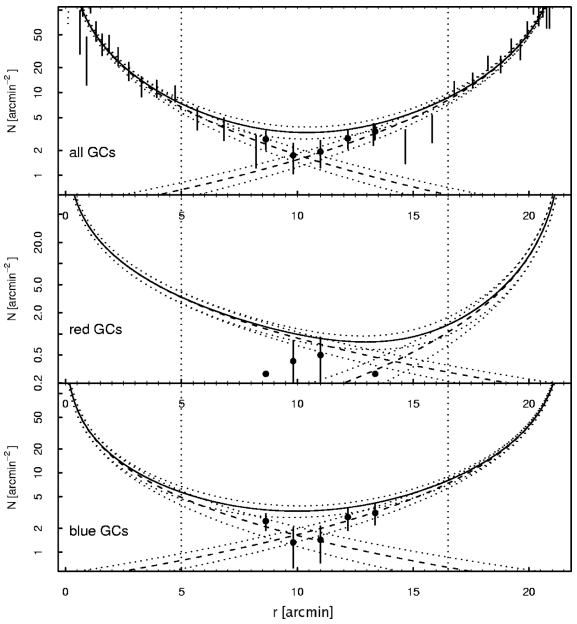


**Figure 16.** Radial densities along the axis connecting both Antlia galaxies, where $r$ is the galactocentric radius measured from NGC 3268 centre. The fits to the radial density profiles of all, red, and blue GCs around NGC 3258 (right-hand side) and NGC 3268 (left-hand side), are extrapolated and compared to the GC density in the 'intracluster' field. Individual GCS profiles are shown with dashed lines and the combined one with a solid line. Dotted lines close to the profiles give their respective errors, and vertical dotted lines show the limits of the FORS1 NGC 3258 and NGC 3268 fields. The 'intracluster' field is divided into five radial ranges whose densities are shown with filled circles. The MOSAIC measurements are included in the upper panel, as vertical solid lines corresponding to the error bars. Please note that vertical scales are different.

all GCs, as well as for reds and blues, are shown in Fig. 16, where NGC 3258 and NGC 3268 would be on the right- and left-hand sides, respectively.

The 'intracluster' field is located on this connecting axis, and we aim at comparing the observed densities in this field with the combined extrapolated profile, along this connecting line. For this reason, the GC densities for five different radial ranges within the 'intracluster' field, completeness corrected and background subtracted, are determined taking a limiting magnitude $V = 25$. The observed densities follow closely the individual extrapolated density profiles (filled circles in Fig. 16). However, number statistics are low as all densities in this field, observed and extrapolated, are below 5 GCs arcmin$^{-2}$. We scaled the MOSAIC densities to those of the VLT fields, which are shown in the upper panel of Fig. 16. On the 'intracluster' field, the combination of the extrapolated fitted functions seems to predict a higher cluster density than the observed one.

If there were some intracluster GCs one would expect the observed density in the 'intracluster' field to be larger than just the sum of the individual GCS extrapolated profiles. The contribution of red GCs is almost negligible, so the analysis is performed basically on the blue ones. Along the axis connecting both galaxies, the range of the observed (blue GC) densities is $1.3 \pm 0.5$–$3.1 \pm 0.6$ arcmin$^{-2}$ while the range of combined (blue GCs) extrapolated densities, within the same radii, is $3.3 \pm 0.6$–$4.2 \pm 0.6$ arcmin$^{-2}$. Though we are dealing with poor number statistics these results suggest that not only the observed densities are not larger than the predicted ones, but they even tend to be smaller.

So far, we do not find from our data any conclusive evidence of the existence of intracluster GCs in the region between NGC 3258 and NGC 3268. However, it should be taken into account that the 'intracluster' field, where there are GCs contributed by both GCSs, has not turn into a proper place to seek for them. We are undertaking a kinematic study of the GC and galaxy content of the Antlia cluster, which will probably help to detect their presence in this cluster.

## 8 SUMMARY AND CONCLUSIONS

On the basis of FORS1/VLT ($V$, $I$) images we have performed an analysis of the GCSs of NGC 3258 and NGC 3268, the dominant elliptical galaxies of the Antlia galaxy cluster. Our first study of these GCSs was based on Washington ($C$, $T1$) photometry and wide-field MOSAIC images (Paper I), which did not reach the TOM of the GCLF. Here we summarize the results and conclusions.

(1) The TOMs of the red, the blue and the total populations are obtained by fitting Gaussians to the respective GCLFs. The distance moduli, obtained from the entire GC sample, are $(m - M) = 32.42 \pm 0.19$ for NGC 3258 and $(m - M) = 32.81 \pm 0.20$ for NGC 3268, which are in good agreement with those obtained by Tonry et al. (2001) via the SBF method. The TOMs of the blue GCs are on the average $\langle \Delta V \rangle = 0.4$ mag brighter than those of the red ones.

(2) The GCLF was independently determined for a field between NGC 3258 and NGC 3268. We could measure a TOM of $V = 24.87 \pm 0.15$ (blue GCs), intermediate between the TOMs of the bright galaxies. This supports the view that we are observing the overlapping of the two GCSs. The actual number density is even somewhat lower than from one would expect by the extrapolation of the number density profiles determined near the host galaxies. We therefore found no evidence of the presence of intracluster GCs in the field between the ellipticals.

(3) The total GC populations are about $6000 \pm 150$ GCs in NGC 3258 and $4750 \pm 150$ GCs in NGC 3268 while the extent of both GCSs is at least 10 arcmin (about 90 kpc). If the relative distances are correct, this corresponds to specific frequencies of $S_N = 8.7 \pm 2.2$ for NGC 3258 and $S_N = 3.7 \pm 0.9$ for NGC 3268.

(4) Other findings from Paper I like the bimodal colour distribution or the azimuthal distributions have been confirmed. The galaxy light profiles match more closely the red GCs radial density profiles. A point not addressed in Paper I is the unimodal colour distribution of the brightest clusters.

The strongest indication so far for the spatial proximity of NGC 3268 and NGC 3258 was the common radial velocity of 2800 km s$^{-1}$. But the GCLF distance moduli rather suggest that NGC 3268 is located somewhat in the background, separated from NGC 3258 by several Mpc. The unusually high specific frequency of NGC 3258 is, however, a rare finding and would ease with a distance equal to that of NGC 3268. A further confirmation would therefore be required. Much evidence suggests that Antlia is a cluster in a very early stage of dynamical evolution, but the spatial and dynamical relationships of its components are still unclear. We started a kinematic study intending to bring more clarity in the understanding of the apparently complex structure of Antlia.

## ACKNOWLEDGMENTS

BD and TR gratefully acknowledge support from the Chilean Centre for Astrophysics FONDAP No. 15010003. LPB is grateful to the

Astronomy Group at the Concepción University, for financial support and warm hospitality during part of this research. This work was also funded with grants from Consejo Nacional de Investigaciones Científicas y Técnicas de la República Argentina, Agencia Nacional de Promoción Científica Tecnológica and Universidad Nacional de La Plata (Argentina).

## REFERENCES

Ashman K. M., Bird C. M., Zepf S. E., 1994, AJ, 108, 2348
Ashman K. M., Conti A., Zepf S. E., 1995, AJ, 110, 1164
Barmby P., Huchra J. P., Brodie J. P., 2001, AJ, 121, 1482
Bassino L. P., Muzzio J. C., Rabolli M., 1994, ApJ, 431, 634
Bassino L. P., Cellone S. A., Forte J. C., Dirsch B., 2003, A&A, 399, 489
Bassino L. P., Faifer F. R., Forte J. C., Dirsch B., Richtler T., Geisler D., Schuberth Y., 2006a, A&A, 451, 789
Bassino L. P., Richtler T., Dirsch B., 2006b, MNRAS, 367, 156
Brodie J. P., Strader J., 2006, ARA&A, 44, 193
Dean J. F., Warren P. R., Cousins A. W. J., 1978, MNRAS, 183, 569
De Bruyne V., De Rijcke S., Dejonghe H., Zeilinger W. W., 2004, MNRAS, 349, 440
Dirsch B., Richtler T., Bassino L. P., 2003a, A&A, 408, 929 (Paper I)
Dirsch B., Richtler T., Geisler D., Forte J. C., Bassino L. P., Gieren W. P., 2003b, AJ, 125, 1908
Dirsch B., Schuberth Y., Richtler T., 2005, A&A, 433, 43
Elson R. A. W., Santiago B. X., 1996, MNRAS, 280, 971
Fellhauer M., Kroupa P., 2005, MNRAS, 359, 223
Ferguson H. C., Sandage A., 1990, AJ, 100, 1
Harris H. C., Canterna R., 1977, AJ, 82, 798
Harris W. E., 2001, in Labhardt L., Binggeli B., eds, Saas-Fee Advanced Course 28, Star Clusters. Springer-Verlag, Berlin, p. 223
Harris W. E., van den Bergh S., 1981, AJ, 86, 1627
Harris W. E., Harris G. L. H., McLaughlin D. E., 1998, AJ, 115, 1801
Harris W. E., Whitmore B. C., Karakla D., Okoń W., Baum W. A., Hanes D. A., Kavelaars J. J., 2006, ApJ, 636, 90
Hopp U., Materne J., 1985, A&AS, 61, 93
Jedrzejewski R. I., 1987, MNRAS, 226, 747
Jordán A., Côtè P., West M. J., Marzke R. O., 2002, ApJ, 576, L113
Jordán A., West M. J., Côtè P., Marzke R. O., 2003, AJ, 125, 1642
Jordán A. et al., 2006, ApJ, 651, L25
Jordán A. et al., 2007, ApJS, 171, 101
Kissler-Patig M., Grillmair C. J., Meylan G., Brodie J. P., Minniti D., Goudfrooij P., 1999, AJ, 117, 1206
Kundu A., Whitmore B. C., 2001, AJ, 121, 2950
Kundu A., Whitmore B. C., Sparks W. B., Macchetto F. D., Zepf S. E., Ashman K. M., 1999, ApJ, 513, 733
Landolt A. U., 1992, AJ, 104, 340
Larsen S. S., Brodie J. P., Huchra J. P., Forbes D. A., Grillmair C. J., 2001, AJ, 121, 2974
McLaughlin D. E., 1994, PASP, 106, 47
Minniti D., Kissler-Patig M., Goudfrooij P., Meylan G., 1998, AJ, 115, 121
Nakazawa K., Makashima K., Fukazawa Y., Tamura T., 2000, PASJ, 52, 623
Ostrov P. G., Forte J. C., Geisler D., 1998, AJ, 116, 2854
Pedersen K., Yoshii Y., Sommer-Larsen J., 1997, ApJ, 485, L17
Prugniel P., Simien F., 1996, A&A, 309, 749
Puzia T. H., Kissler-Patig M., Brodie J. P., Huchra J. P., 1999, AJ, 118, 2734
Reid N., Boisson C., Sansom E. A., 1994, MNRAS, 269, 713
Rhode K. L., Zepf S. E., 2001, AJ, 121, 210
Rhode K. L., Zepf S. E., 2004, AJ, 127, 302
Richtler T., 2003, in Alloin D., Gieren W., eds, Lecture Notes in Physics Vol. 635, Stellar Candles for the Extragalactic Distance Scale. Springer, Berlin, p. 281
Richtler T., 2006, Bull. Astron. Soc. India, 34, 83
Rieke G. H., Lebofsky M. J., 1985, ApJ, 288, 618
Schlegel D. J., Finkbeiner D. P., Davis M., 1998, ApJ, 500, 525
Spitler L. R., Larsen S. S., Strader J., Brodie J. P., Forbes D. A., Beasley M. A., 2006, AJ, 132, 1593
Stanek K. Z., 1996, ApJ, 460, L37
Strader J., Brodie J. P., Spitler L., Beasley M. A., 2006, AJ, 132, 2333
Tonry J. L., Dressler A., Blakeslee J. P., Ajhar E. A., Fletcher A. B., Luppino G. A., Metzger M. R., Moore C. B., 2001, AJ, 546, 681
West M. J., Côtè P., Jones C., Forman W., Marzke R. O., 1995, AJ, 453, L77
Williams B. F. et al., 2007, ApJ, 654, 835
Yahagi H., Bekki K., 2005, MNRAS, 364, L86

This paper has been typeset from a TEX/LATEX file prepared by the author.